SEMARAK ILMU PUBLISHING

Journal of Advanced Research in Applied Mechanics

Journal homepage:
https://semarakilmu.com.my/journals/index.php/appl_mech/index
ISSN: 2289-7895

Validation Calibration Factor of Single Photon Emission Computed Tomography for Iodine-131 using Non-Spherical Targeted Volume

Mohd Akmal Masud[1,4], Mohd Zamani Ngali[2,*], Siti Amira Othman[1], Ishkrizat Taib[2], Kahar Osman[3], Salihatun Md Salleh[2], Ahmad Zahran Md. Khudzari[3], Nor Salita Ali[4], Anucha Chaichana[5]

[1] Faculty of Applied Sciences and Technology, Universiti Tun Hussein Onn Malaysia, 84600 Panchor, Johor, Malaysia
[2] Faculty of Manufacturing and Engineering, Universiti Tun Hussein Onn Malaysia, 86400 Batu Pahat Johor, Malaysia
[3] Faculty of Biosciences and Medical Engineering, Universiti Teknologi Malaysia, 81310 Johor Bahru, Johor, Malaysia
[4] Nuclear Medicine Department, National Cancer Institute, 62250 Putrajaya, Malaysia
[5] Faculty of Medical Technology, Department of Radiological Technology, Mahidol University, Bangkok 10700, Thailand

ARTICLE INFO

Article history:
Received 22 June 2023
Received in revised form 24 August 2023
Accepted 9 September 2023
Available online 18 October 2023

Keywords:
SPEC; calibration factor; quantitative

ABSTRACT

Absolute quantification of Iodine-131 (^{131}I) on Single Photon Emission Computed Tomography (SPECT) imaging is extremely necessary for the lesion dose per administrative differentiated thyroid cancer procedure. However, non-quantitative SPECT imaging makes determining the dose required for a tumour to be treated is challenging. This multi-vendor and multi-centre research use phantom measures to assess the quantitative accuracy and inter-system variability of various SPECT/CT systems. Hence, this study aims to determine the calibration factor (CF) for ^{131}I activity quantification using the National Electrical Manufacturer Association (NEMA) phantom uptake for the Philips BrightView XCT modality. The accuracy activity concentration for a non-spherical targeted volume is less than 15% compared to a spherical targeted volume (<9%). Furthermore, the CF has no significant difference in the value between the matrix sizes of 64×64, 128×128, and 256×256. Therefore, the gamma camera CF must be precisely determined to convert the reconstructed images' counts into activity values for quantitative imaging. However, the NEMA phantom with spherical geometrical is the standard tool for determining CF, the various geometrical shapes other than spherical should be considered for determining CF because the effect of photon distribution contribution is different for any different lesion geometrical.

1. Introduction

In current years, the interest and importance of radiopharmaceutical distribution quantification have manifested remarkable utilization in clinical trials, especially those related to Single Photon Emission Computed Tomography (SPECT) [1]. In particular, SPECT can be advantageous for measuring the reserve of myocardial blood flow, diagnosis of multivessel diseases, and quantitative assessment

* *Corresponding author.*
E-mail address: zamani@uthm.edu.my

https://doi.org/10.37934/aram.110.1.7385

of the kidneys, brain, lungs, and other organs. Moreover, activity quantitation plays a leading role in targeted radionuclide therapies, specifically in personalized medicine [2].

In general, Iodine-131 (^{131}I) is widely used to diagnose thyroid disorders, including hypothyroidism and differentiated thyroid carcinoma [3]. Subsequently, the most prevalent endocrine malignant tumour is thyroid cancer, with accelerating occurrence [4]. The most common orally administered method concerning ^{131}I therapy revealing benign thyroid disease is 69.1%, while another 26.6% of the signs are for malignant diseases [5]. The lesion dose per administrator for ^{131}I can be calculated using SPECT scans, which can be just as quantitative as Positron Emission Tomography (PET) scans. To obtain SPECT images, standard corrections must be made for photon scattering and attenuation, instrumental dead time, resolution recovery, cross-calibration, and radioactive decay in units of kBqml^{-1} [6–8].

Traditionally, SPECT ^{131}I imaging is considered non-quantitative [9]. However, quantitative SPECT is now possible like PET due to developments in multimodality SPECT, image reconstruction algorithms, and opulent correction techniques to compensate for photon attenuation and dispersion (e.g., kBqcm^{-3} standardized uptake value). Analysis of the quantitative SPECT evidence showed clinical studies where the reliability of the retrieved SPECT data was tested *in vivo* [8]. The sensitivity (count rate per unit activity) of a specific gamma camera (SPECT collimator) was constant. Over the same period, radioactive sources with greater radioactivity can increase the overall count in the planar image. In other words, radioactivity affects the value of time acquisition [10].

The next element that needs to be considered when performing SPECT quantification is the partial-volume effect (PVE) or the recovery coefficient (R.C). This is the most essential yet difficult modification in quantitative SPECT imaging [11]. The apparent volume to true volume ratio is known as the R.C. After quantification, it can be used to modify the activity of tiny structures. Note that the SPECT subpar spatial resolution brings this on.

However, the existing research efforts mainly focus on quantification using spherical targeted volume [12–15] rather than non-spherical targeted volume. More advanced calibration factors (CF) have to be advised for objects not properly approximated as spheres since R.C. depends on the target volume and other parameters, such as the target shape [16]. In contrast, the shape of the lesions is different, and the structure is complex, especially the small area and high density of bone metastases, bringing great challenges to the reliable quantification of lesions [17].

To validate the CF for non-spherical targeted volume, this study aimed to obtain the absolute CF for ^{131}I to convert the counts to activity in Megabecquerel (MBq). In addition, this study wants to know whether it has a different CF between the dimensions of 64, 128, and 256. The quantitative exactness of the R.C and inter-system variability were calculated using different phantom experiments. Other than that, the effects of different projection collections in non-spherical targeted volumes using custom-made shapes were analyzed. The results of these CFs represent the first step of our preliminary study as a single-experience cancer centre for calculating lesion dosimetry [18].

2. Methodology

A National Electrical Manufacturers Association (NEMA) phantom was utilized to simulate lesions [14]. This phantom consists of 6 spheres inserted with volumes for each sphere of 26.65 mL, 11.5 mL, 5.6 mL, 2.7 mL, 1.1 mL, and 0.52 mL, respectively. A Single Photon Emission Computed Tomography (SPECT) scanner (BrightView XCT) was employed for image reconstruction. Note that a high-energy general-purpose collimator is also applied for the two opposite detectors.

2.1 Phantom Preparation

Using a Philips BrightView XCT scanner, the International Electrotechnical Commission (IEC) Body Phantom of the NEMA was scanned [19]. Many experts advise utilizing the NEMA IEC body phantom for whole-body SPECT imaging. Six volumes of interest (VOI) on the spheres of this phantom, each with a different diameter, were measured. The inner diameters of these phantoms were 10, 13, 17, 22, 28, and 37 mm. According to Figure 1, the VOI was scaled to the physical sphere's inner diameter.

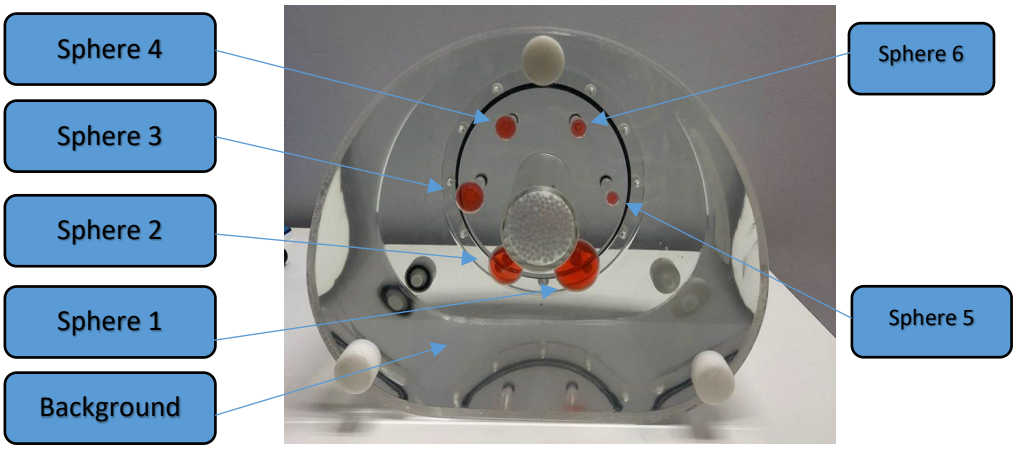

Fig. 1. NEMA IEC body phantom

A 1000-litre glass bottle containing 212 Megabecquerel Iodine-131 (MBq ^{131}I) will be used as the activity concentration sphere [20]. For the first scan, the activity concentration was 0.212 MBqml^{-1} (Table 1 followed until the fourth scan, as reported in Table 1). There were six different geometries of spheres, each containing 0.212 MBqml^{-1}. For the first scan of six spheres, the initial activity is 5.22 MBq, 2.23 MBq, 1.03 MBq, 0.51 MBq, 0.26 MBq, and 0.11 MBq, respectively, for inner sphere diameters of 37 mm, 28 mm, 22 mm, 17 mm, and 13 mm. The phantom included radiopharmaceuticals and weighed 12 kg. On the other hand, the MATLAB R2022a program calculated the spheres' volume and numbers (Mathworks Inc., Sherborn, MA, USA).

Based on the NEMA NU 2-2007 standard, the activity of the concentration background region was filled with 0.0210 MBqml^{-1} ^{131}I (NEMA Standards Publication NU 2-2012, 2013). Therefore, the ratio of the sphere to the background is 10:1.

Table 1
The activity concentration of the sphere from 1st scan until 4th scan

No. of Scan	Sphere Concentration (MBqml^{-1})	Background Concentration (MBqml^{-1})
1st scan	0.212	0.0217
2nd scan	0.097	0.0098
3rd scan	0.058	0.0059
4th scan	0.029	0.0031

2.2 SPECT Calibration Factor Determination

The counts accumulated in the sphere phantom have been determined using MATLAB R2022a software [21]. First, the counts in each sphere were calculated by percentage due to maximum counts. This means the maximum counts in each sphere will be multiplied by a certain percentage until the actual volume of each sphere is reached. Consequently, the function *interp3* was used for

fusing image computed tomography (CT) and SPECT, and then the *isosurface* function was developed for three-dimensional (3D) viewing, as shown in Figure 2.

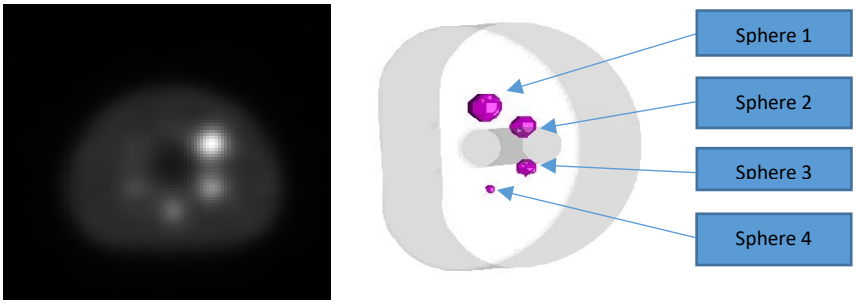

Fig. 2. Three-dimensional SPECT/CT images

The CF of ^{131}I has been calculated utilizing the following equation given in Eq. (1), where counts per second (cps) are divided by known activity (MBq) [22]. The CF was calculated separately for the six spherical dimensions: 64×64, 128×128, and 256×256. Simultaneously, the cps can be obtained from the ratio of the time acquisition (*At*) to the total counts in the sphere. On the other hand, known activity is the activity of ^{131}I in MBq ^{131}I units.

$$CF = \frac{counts\ per\ seconds\ (cps)}{activity\ (MBq)} \tag{1}$$

Recovery coefficients (R.C) were calculated to measure the underestimating of activity because of activity spilling outside the sphere's limits as follows:

$$RC = \frac{As}{At} \tag{2}$$

where *As* represents the activity measured in the spheres, while *At* is the actual activity filling the spheres.

2.3 SPECT Data Acquisition and Reconstruction

As shown in Figure 2, all acquisition phantoms were done utilizing a high-energy general-purpose (HEGP) parallel-hole collimator and a Philips BrightView XCT with CT capability [23]. With pixel sizes of 9.32, 4.64, and 2.33 mm, respectively, three matrix sizes—64x64, 128x128, and 256x256—were examined. Note that 40 viewing angles covering 360° and a scatter correction window of 364 keV 10% were employed for each matrix size.

Using a body-contouring detection technique [24, 25], the phantom was placed in the middle of the area and close to the detector. The collimator was positioned with detectors 1 and 2 having radii of 33 cm respectively, and the step-and-shoot scan mode was set to 40 s/frame. To adjust for attenuation and pinpoint the subject's precise location within the phantom during image processing, an attenuation-corrected CT scan having an energy of 120 kV and a tube current of 20 mAs was utilized. The first, second, third, and fourth scans all had identical SPECT measurements with concentrations of 0.212 MBqml^{-1}, 0.097 MBqml^{-1}, 0.058 MBqml^{-1}, and 0.029 MBqml^{-1}, respectively.

To rebuild the recorded SPECT pictures, a 3D ordered-subset expectation maximization (OSEM) algorithm was used. The number of iterations used is 2 with a fixed subset(s) of 8, which is a clinical

diagnostic standard. This setting was reconstructed by applying all three matrix sizes: 64×64, 128×128, and 256×256.

2.4 Calibration Factor Validation for Iodine-131

To validate the calibration of ^{131}I, three shapes were custom-made into the liver, kidney, and spleen shapes, but the volume is the same as the spheres 26.65 mL, 5.5 mL and 11.5 mL, while the three-sphere, whose volumes are 26.65 mL, 11.5 mL, and 5.5 mL, was maintained. The purpose of another shape is to determine whether the different shapes have the same volume and activity, and the CF can calculate the real activity. In clinical diagnostic practice, the phantom was scanned three times to obtain average readings for only 128×128 dimensions. Hence, MATLAB R2022a software was used to measure the volume and counts (MathWorks Inc., Sherborn, MA, USA). The personalized, targeted volume is shown in Figure 3.

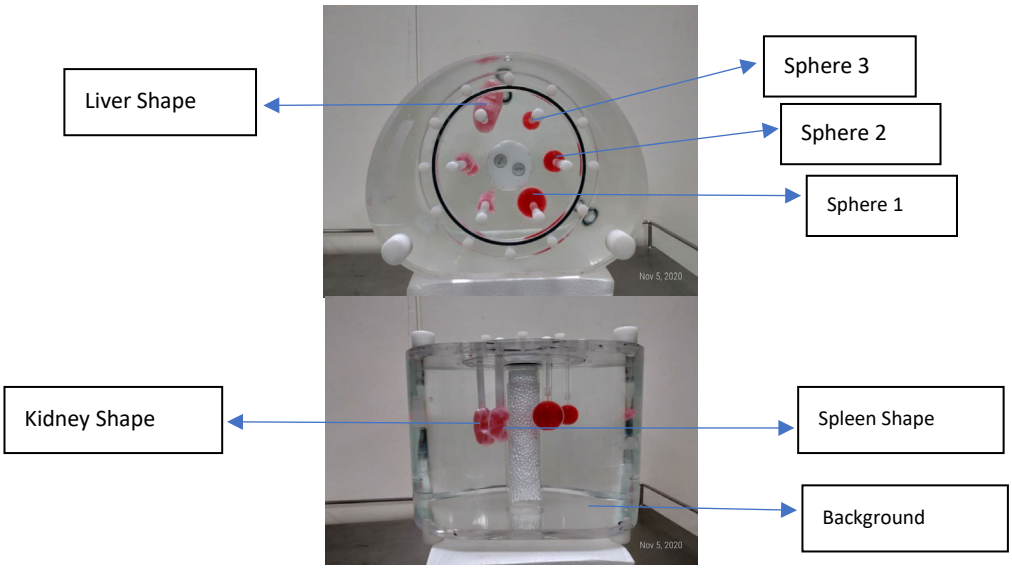

Fig. 3. Customize volume targeted

3. Results

Table 2, 3 and 4 show the counts per second (cps) and the volume of each sphere calculated for images with the dimensions of 64x63, 128x128 and 256x256, respectively. Table 2 shows four scans made for the dimension size 64x64. The cps and volume can be calculated only for the four largest spheres because the concentration volume of spheres 5 and 6 is almost the same as the background concentration. Nevertheless, it can be observed that the cps for sphere 1 shows the highest cps reading for each dimension of 64x64, 128x128 and 256x256, which are 287.42 cps, 280.69 cps and 319.89 cps, respectively.

For the volume, all volumes calculated from the 1st to the 4th scans do not exceed the actual volume for spheres 1 to 4. Therefore, for known activity (MBq), the concentration of the 1st scanning from Table 1 will be multiplied by the volume calculated for each sphere for each dimension. Likewise, with the 2nd, 3rd and 4th scanning, all known activities obtained from the concentration of each scanning in Table 1 will be multiplied by the volume of each sphere.

Table 2
Data for dimension 64×54

No. of Scan	No. of Sphere	Known Activity (MBq)	Counts per Second (CPS)	Volume/mL
1st Scan	SPHERE 1	5.34	287.42	25.16
	SPHERE 2	2.24	83.73	10.55
	SPHERE 3	1.03	31.79	4.87
	SPHERE 4	0.52	13.30	2.43
2nd Scan	SPHERE 1	2.29	137.44	23.54
	SPHERE 2	0.87	32.92	8.93
	SPHERE 3	0.47	14.88	4.87
	SPHERE 4	0.16	3.95	1.62
3rd Scan	SPHERE 1	1.32	80.08	22.73
	SPHERE 2	0.66	28.16	11.36
	SPHERE 3	0.24	7.95	4.06
	SPHERE 4	0.09	2.55	1.62
4th Scan	SPHERE 1	0.68	43.69	23.54
	SPHERE 2	0.33	13.13	11.36
	SPHERE 3	0.14	4.49	4.87
	SPHERE 4	0.05	1.20	1.62

Table 3
Data for dimension 128×128

No. of Scan	No. of Sphere	Known Activity (MBq)	Counts per Second (cps)	Volume/mL
1st Scan	SPHERE 1	4.83	280.69	22.83
	SPHERE 2	2.30	85.66	10.86
	SPHERE 3	0.90	26.99	4.26
	SPHERE 4	0.56	13.63	2.64
2nd Scan	SPHERE 1	2.22	138.25	22.83
	SPHERE 2	0.98	38.27	10.04
	SPHERE 3	0.48	15.00	4.97
	SPHERE 4	0.24	6.26	2.43
3rd Scan	SPHERE 1	1.77	77.52	22.22
	SPHERE 2	0.92	22.88	9.84
	SPHERE 3	0.71	9.76	5.07
	SPHERE 4	0.62	3.82	2.43
4th Scan	SPHERE 1	0.77	43.56	26.48
	SPHERE 2	0.27	11.23	9.44
	SPHERE 3	0.14	4.58	4.87
	SPHERE 4	0.08	2.23	2.64

Table 4
Data for dimension 256x256

No. of Scan	No. of Sphere	Known Activity (MBq)	Counts per Second (cps)	Volume/mL
1st Scan	SPHERE 1	5.42	319.89	25.62
	SPHERE 2	2.33	87.59	11.03
	SPHERE 3	1.15	32.84	5.42
	SPHERE 4	0.53	12.88	2.49
2nd Scan	SPHERE 1	2.46	148.48	25.31
	SPHERE 2	0.91	33.30	9.33
	SPHERE 3	0.46	13.53	4.74
	SPHERE 4	0.36	9.47	3.75
3rd Scan	SPHERE 1	1.48	87.03	25.48
	SPHERE 2	0.60	20.79	10.36
	SPHERE 3	0.24	7.69	4.11
	SPHERE 4	0.07	2.15	1.28
4th Scan	SPHERE 1	0.74	44.07	25.60
	SPHERE 2	0.29	10.71	10.16
	SPHERE 3	0.12	3.55	4.30
	SPHERE 4	0.06	1.44	2.17

To obtain the Single Photon Emission Computed Tomography (SPECT) calibration factor (CF), a cps graph on the x-axis and known activity (MBq) on the y-axis are plotted for each dimension, as shown in Figure 4 a, b and c. From the graph, we can see that the gradient is representative of CF for SPECT. For dimensions 64x64, 128x128 and 256x256, we obtain 0.0163 $cpsMBq^{-1}$, 0.167 $cpsMBq^{-1}$ and 0.165 $cpsMBq^{-1}$, respectively. Note that the intercept shows an increase from 64x64, 128x128 and 256x256 dimensions, which are 0.1485 cps, 0.1911 cps and 0.2167 cps, respectively.

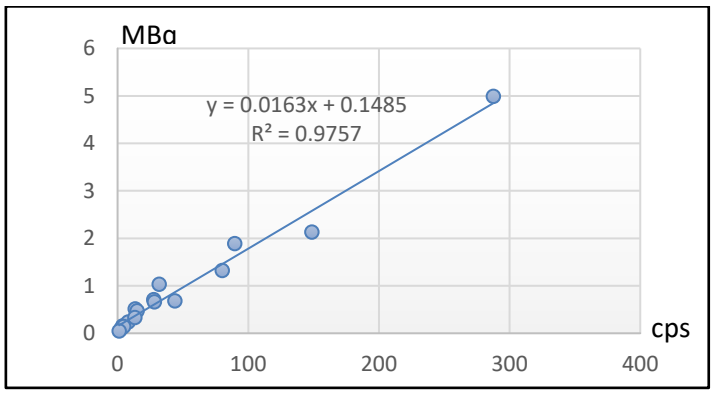

(a)

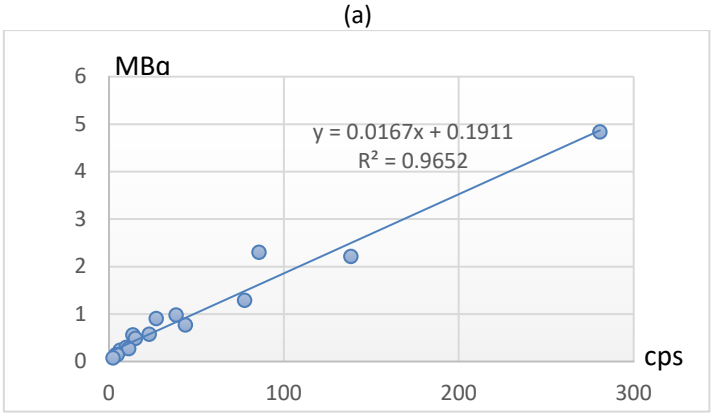

(b)

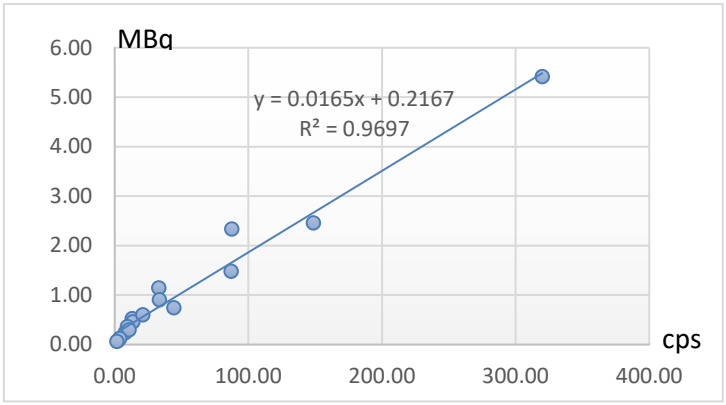

(c)

Fig. 4. (a) 64x64 dimensionc alibrationf actor (b) 128x128 graph calibration factor (c) 256x256 graph calibration factor

It is noteworthy that the CF is constant for every matrix size used. Regarding the calculation of the CF ^{131}I, as shown in Figure 5, there were no significant changes in the ^{131}I CF for different cps in every sphere. As for sensitivity, it shows an increasing trend for matrix sizes 64x64, 128x128 and 256x256, which are 0.1485 cps, 0.1911 cps and 0.2167 cps, respectively. This shows that the smaller the size of pixel images, the more sensitive the collection counts on each pixel, making the value of pixel counts higher.

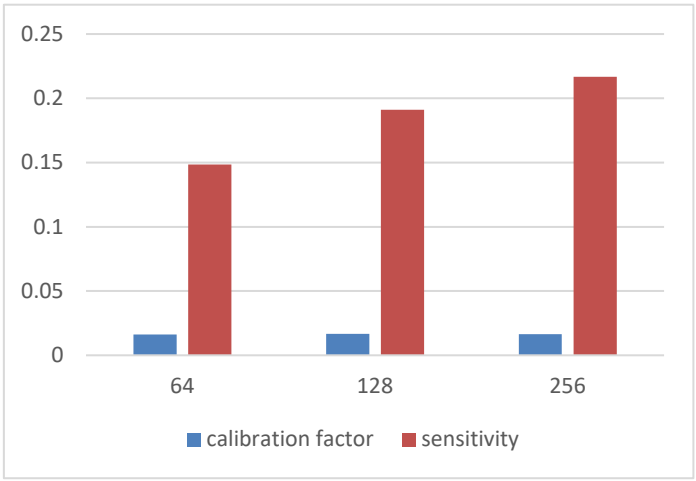

Fig. 5. Calibration Factor and sensitivity bar chart

For instance, employing a reasonable amount of iterations, the recovery coefficient (R.C) turned out to be less than 0.8 for sphere volumes of less than 11 mL in the ^{131}I phantom data shown in Figure 6. If R.C. is not used in this situation, activity quantification errors in such volumes will surpass 20%. More advanced partial-volume correction methods are available for objects not properly approximated as spheres and are advised because R.C. depends on the target volume and other aspects like the targeted shape. In any event, for volumes less than about 8 mL, a significant error in activity estimations can be predicted due to the poor ^{131}I SPECT resolution (1.3 cm in full width at half maximum at 10 cm) (or diameters of 2.5 cm, which is less than twice the full width at half maximum). Consequently, the predictions for these volumes should be utilized with caution.

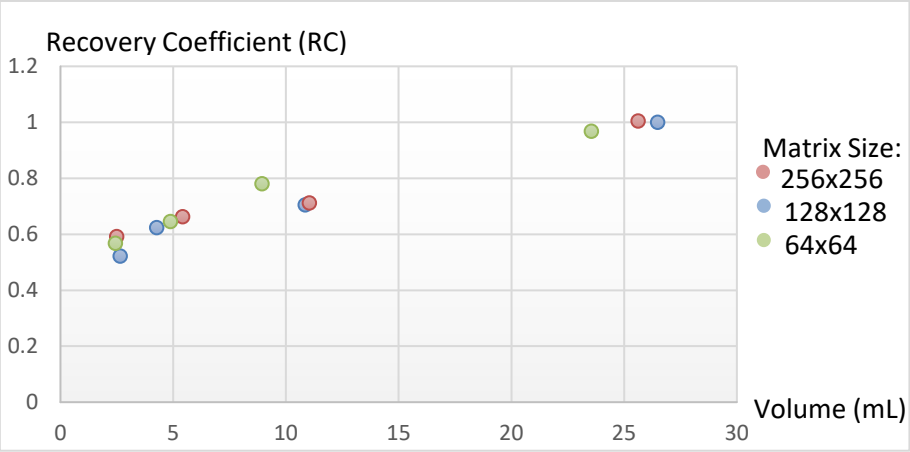

Fig. 6. R.C as a function of volume at 8 iteration

For the validation of the CF, as shown in Table 5, sphere 1 (26.65 mL) has a percentage deviation of 0.07%, sphere 2 (11.53 mL) has a percentage deviation of -8.42%, and sphere 3 (5.99 mL) has a percentage deviation of -6.25%. For the custom-made phantom, for the liver shape (26.61 mL), the percentage deviation was 12.57%. Meanwhile, for the kidney shape (11.38 mL), the percentage deviation was -4.66%, while for the spleen shape (5.82 mL), the percentage deviation was -0.72%. All data are shown in Table 5.

Following the three different volumes in the background shown in Table 5 (Background 1, Background 2, Background 3), the percentage deviation is around 58% to 75% despite the number of cps being in the range calibrated. This is because the volumes of the three background volumes are not in range as the volume is calibrated. Therefore, if this CF is applied, the cps is higher or lower than the cps mentioned, and the volume is not in the range mentioned, so the percentage deviation is more than 30%.

It also shows that the background's activity concentration was not in the calibrated range of activity concentration, as mentioned in Table 1. It is known that the filled activity concentration for the background is 0.015 MBq.ml^{-1}, whereas the calibrated activity concentration ranges from 0.212 to 0.029 MBq.ml^{-1}, as mentioned in Table 1.

Remarkably, the result is in concordance with [20], who stated that the best radionuclide for SPECT quantification is Technitium-99m (Tc-99m), followed by Lutetium-177 (Lu-177) and ^{131}I. This is because Tc-99m emitted a gamma energy of 140 keV, and the scintillation detector is technically suitable for 140 keV gamma rays.

In addition, although the concentration and activity of ^{131}I in the sphere changed, the CF did not change. In addition, there was no significant difference in the CF for ^{131}I between the different matrix sizes of 64×64, 128×128, and 256×256. All these results are significantly aligned with other research [1, 26, 27], and if the matrix size changes, the CF does not change because the counts collected in the Digital Imaging and Communications in Medicine (DICOM) information are the same detector.

However, dimensions 256×256 are more accurate for the R.C. of the volume calculation in comparison to dimensions 128×128 and 64×64. This is because the pixel size for dimensions 256×256 is 2.13 mm compared to dimensions 128×128 and 64×64, which are 4.64 mm and 9.332 mm, respectively.

Table 5
Distribution data of validation calibration factor

Geometrical Sphere	Volume/mL	Counts per Second/cps	Known Activity (Mbq)	Activity Calculation (Mbq)	% Deviation
SPHERE 1	26.62	204.06	3.99	4.00	0.07
LIVER	26.61	245.35	3.99	4.57	12.57
SPHERE 2	11.53	57.33	1.73	1.60	-8.42
KIDNEY	11.38	59.12	1.71	1.63	-4.66
SPHERE 3	5.99	23.84	0.90	0.85	-6.25
SPLEEN	5.82	24.67	0.87	0.87	-0.72
BACKGROUND 1	185.00	420.59	2.78	6.74	58.84
BACKGROUND 2	57.36	130.08	0.86	2.89	70.18
BACKGROUND 3	27.00	59.95	0.41	1.65	75.42

In this study, only the sphere-to-background with a ratio of 10:1 was utilized. Therefore, only spheres 1, 2, 3, and 4 appear when the threshold is set to obtain the actual volume. This is because the counts in spheres 5 and 6 were the same as the cps in the background. Therefore, if the threshold is set to obtain the actual volume for spheres 5 and 6, the volumes of spheres 5 and 6 are combined with the background volume. Thus, this is a limitation of the present study.

In addition, the study did not discuss a segmentation method to obtain the volume of the sphere. Instead, the count threshold for every sphere was set individually to obtain the actual volume until the actual volume was obtained.

For the CF calculation, some other studies used the mean cps of the sphere separated by the sphere's known activity concentration. The equation [6] can be written as:

$$CF = \frac{(counts/no.voxel)/acquisition\ time\ (mean\ cps)}{activity\ concentration\ \left(\frac{MBq}{ml}\right)} \tag{3}$$

However, when this equation is applied to obtain the CF for every sphere, the result is identical to that shown in Eq. (1). Thus, using total counts per second or mean cps still provides a similar CF.

For graph R.Cs of the three dimensions, 64×64, 128×128, and 256×256, it was revealed that the trendline R.C of all dimensions was changed for all scans. This is because the activity concentration changes owing to the half-life of ^{131}I. For the custom-made liver, kidney, and spleen, even though the shape is not a sphere, the percentage deviation is still below 15%. Nevertheless, it was slightly higher for the percentage deviation liver, which was approximately 12% of the other custom-made shapes. This is because the width (diameter) of the liver is greater than the diameter of sphere 1. Therefore, the collected maximum counts in the centre of the liver were greater than the maximum counts in sphere 1.

On that note, this result is identical to the study done by [8, 26, 28, 29]. Despite using up to 100 mL for the sphere in the experiment, the study's findings indicate that ^{131}I still needed the R.C to obtain almost actual activity in the lesion. However, a study by [9, 13] tested Tc-99m quantification. In these findings, the cut-off volume is not needed for the R.C to obtain the actual activity. The main difference between ^{131}I and Tc-99 is the energy windows.

In addition, Tc-99 is more sensitive than ^{131}I because the energy of Tc-99 is 140 keV compared to ^{131}I, which is 364 keV. Remarkably, the studied spec SPECT detector is much more sensitive to gamma rays ranging between 120 and 140 keV.

In future studies, the CF of ^{131}I with several different geometrical shapes, such as the spleen, kidney, and liver, will be validated. The CF is critically used for the absorbance of dose calculation in

tumours and organs at risk for internal dosimetry. Apart from that, the findings imply that more realistic geometries should be used to analyze the coefficients for recovery of partial-volume correction, which are usually evaluated in spherical geometries.

4. Conclusions

A three-dimensional (3D) gamma camera that has a high-energy collimator from a commercial Single Photon Emission Computed Tomography (SPECT), as well as a workstation for processing images employing a six-sphere National Electrical Manufacturers Association (NEMA) phantom, has been used to quantify thyroid uptake of Iodine-131 (^{131}I) radioactive activity. With the scattered and background contributions eliminated, the SPECT calibration factor (CF) may be calculated using various geometrical NEMA phantoms. However, this straightforward strategy still yields a CF with enough accuracy of less than (~ 15%) to be used in clinical diagnosis for radiotracer quantification. Other than that, accurate and precise SPECT provides a better understanding of the distribution of radiopharmaceuticals for estimating standard target organ doses. In addition, the long-term goal is to compare the CF using non-spherical geometries, such as the ellipse shape and the ideal distance source, to investigate more applications of the best ^{131}I lesion volume segmentation method. This promoted method works perfectly for a background ratio of 10:1 to the target lesion. However, as the background increases, the border of the target sphere fades into the background and blends into it. In other terms, this CF calculation is practically fit only for a crystal detector of 9.5 mm thickness.

Acknowledgement

The authors would like to thank the Director General of Health Malaysia for the permission to publish this paper and want to express gratitude to Institut Kanser Negara for the facilities provided. The funding for the project has been provided by Kementerian Pengajian Tinggi Malaysia (KPTM) under the FRGS grant (Grant No: FRGS/1/2019 Vot K200) that made the research possible. Ethical approval for this study was obtained from the Medical Research and Ethics Committee (MREC), Ministry of Health Malaysia (NMRR-20-1239-53306).

References

[1] Zhao, Wei, Pedro L. Esquinas, Xinchi Hou, Carlos F. Uribe, Marjorie Gonzalez, Jean-Mathieu Beauregard, Yuni K. Dewaraja, and Anna Celler. "Determination of gamma camera calibration factors for quantitation of therapeutic radioisotopes." *EJNMMI physics* 5 (2018): 1-16. https://doi.org/10.1186/s40658-018-0208-9

[2] Ashhar, Zarif, Nor Azah Yusof, Fathinul Fikri Ahmad Saad, Siti Mariam Mohd Nor, Faruq Mohammad, Wan Hamirul Bahrin Wan Kamal, Muhammad Hishar Hassan, Hazlina Ahmad Hassali, and Hamad A. Al-Lohedan. "Preparation, characterization, and radiolabeling of [68Ga] Ga-NODAGA-Pamidronic acid: a potential PET bone imaging agent." *Molecules* 25, no. 11 (2020): 2668. https://doi.org/10.3390/molecules25112668

[3] Yahya, MH Mohd, F. N. A. Halim, and S. Mansor. "Validation of 131I activity in thyroid phantom using SPECT/CT 3D image based dosimetry." In *Journal of Physics: Conference Series*, vol. 1497, no. 1, p. 012031. IOP Publishing, 2020. https://doi.org/10.1088/1742-6596/1497/1/012031

[4] Kim, Youjin, Jonghwan Hyeon, Kyo-Joong Oh, and Ho-Jin Choi. "Medical prognosis generation from general blood test results using knowledge-based and machine-learning-based approaches." In *AI 2016: Advances in Artificial Intelligence: 29th Australasian Joint Conference, Hobart, TAS, Australia, December 5-8, 2016, Proceedings 29*, pp. 125-136. Springer International Publishing, 2016. https://doi.org/10.1007/s13244-016-0474-9

[5] Klaassen, Nienke JM, Mark J. Arntz, Alexandra Gil Arranja, Joey Roosen, and J. Frank W. Nijsen. "The various therapeutic applications of the medical isotope holmium-166: a narrative review." *EJNMMI radiopharmacy and chemistry* 4, no. 1 (2019): 1-26. https://doi.org/10.1186/s41181-019-0066-3

[6] Bailey, Dale L., and Kathy P. Willowson. "An evidence-based review of quantitative SPECT imaging and potential clinical applications." *Journal of nuclear medicine* 54, no. 1 (2013): 83-89. https://doi.org/10.2967/jnumed.112.111476

[7] Braghirolli, Ana Maria S., William Waissmann, Juliana Batista da Silva, and Gonçalo R. dos Santos. "Production of iodine-124 and its applications in nuclear medicine." *Applied Radiation and isotopes* 90 (2014): 138-148. https://doi.org/10.1016/j.apradiso.2014.03.026

[8] Bailey, Dale L., and Kathy P. Willowson. "Quantitative SPECT/CT: SPECT joins PET as a quantitative imaging modality." *European journal of nuclear medicine and molecular imaging* 41 (2014): 17-25. https://doi.org/10.1007/s00259-013-2542-4

[9] Ferrando, Ornella, Alessandro Chimenz, Franca Foppiano, and Andrea Ciarmiello. "SPECT/CT activity quantification in 99mTc-MAA acquisitions." *Journal of Diagnostic Imaging in Therapy* 5, no. 1 (2018): 32-36. https://doi.org/10.17229/jdit.2018-0624-034

[10] Roach, Paul J., Geoffrey P. Schembri, and Dale L. Bailey. "V/q scanning using SPECT and SPECT/CT." *Journal of nuclear medicine* 54, no. 9 (2013): 1588-1596. https://doi.org/10.2967/jnumed.113.124602

[11] "EANM'17: Annual Congress of the European Association of Nuclear Medicine"*European Journal of Nuclear Medicine and Molecular Imaging* 44, no. Suppl.2 (2017): 119–956. https://doi.org/10.1007/s00259-017-3822-1

[12] Demir, Mustafa, Mohammad Abuqbeitah, Nami Yeyin, and Kerim Sönmezoğlu. "Comparison between PET/MR and PET/CT: NEMA tests and image quality." *Turkish Journal of Oncology* 32, no. 3 (2017). https://doi.org/10.5505/tjo.2017.1599

[13] Gnesin, Silvano, Paulo Leite Ferreira, Jerome Malterre, Priscille Laub, John O. Prior, and Francis R. Verdun. "Phantom validation of Tc-99m absolute quantification in a SPECT/CT commercial device." *Computational and mathematical methods in medicine* 2016 (2016). https://doi.org/10.1155/2016/4360371

[14] Jenkins, Lee, Erin Ross, Antti Sohlberg, and Peter Esser. "A new SUV phantom for SPECT and PET." (2016): 592-592.

[15] Van Gils, C. A. J., C. Beijst, R. Van Rooij, and H. W. A. M. De Jong. "Impact of reconstruction parameters on quantitative I-131 SPECT." *Physics in Medicine & Biology* 61, no. 14 (2016): 5166. https://doi.org/10.1088/0031-9155/61/14/5166

[16] Zimmerman, Brian E., Darko Grošev, Irène Buvat, Marco A. Coca Pérez, Eric C. Frey, Alan Green, Anchali Krisanachinda et al. "Multi-centre evaluation of accuracy and reproducibility of planar and SPECT image quantification: an IAEA phantom study." *Zeitschrift für Medizinische Physik* 27, no. 2 (2017): 98-112. https://doi.org/10.1016/j.zemedi.2016.03.008

[17] López, A., R. Reynosa, A. Palau, J. M. Martín, J. Castillo, L. A. Torres, and F. Batle. "Gamma cameras calibration for I-131 uptake quantification in Hyperthyroidism diseases." In *World Congress on Medical Physics and Biomedical Engineering, June 7-12, 2015, Toronto, Canada*, pp. 699-703. Springer International Publishing, 2015. https://doi.org/10.1007/978-3-319-19387-8_172

[18] Peters, Steffie, Sebastiaan L. Meyer Viol, Niels R. van der Werf, Nick de Jong, Floris HP van Velden, Antoi Meeuwis, Mark W. Konijnenberg, Martin Gotthardt, Hugo WAM de Jong, and Marcel Segbers. "Variability in lutetium-177 SPECT quantification between different state-of-the-art SPECT/CT systems." *EJNMMI physics* 7, no. 1 (2020): 1-13. https://doi.org/10.1186/s40658-020-0278-3

[19] Dimitrovski, Ivica, Dragi Kocev, Ivan Kitanovski, Suzana Loskovska, and Sašo Džeroski. "Improved medical image modality classification using a combination of visual and textual features." *Computerized Medical Imaging and Graphics* 39 (2015): 14-26. https://doi.org/10.1016/j.compmedimag.2014.06.005

[20] Said, M. A., M. A. Masud, and Abdul Razak HR. "Quantitative imaging with commercial SPECT." In *Journal of Physics: Conference Series*, vol. 1497, no. 1, p. 012025. IOP Publishing, 2020. https://doi.org/10.1088/1742-6596/1497/1/012025

[21] Chaichana, A., and C. Tocharoenchai. "Development of a software tool for an internal dosimetry using MIRD method." In *Journal of Physics: Conference Series*, vol. 694, no. 1, p. 012056. IOP Publishing, 2016. https://doi.org/10.1088/1742-6596/694/1/012056

[22] Carvalho, Samira Marques, Ana Paula Marques Costa, Celso Dario Ramos, Sérgio Querino Brunetto, and Daniel Alexandre Baptista Bonifácio. "Impact of the counts density of calibration image and the image reconstruction parameters in 131I SPECT image quantification." *Brazilian Journal of Radiation Sciences* 6, no. 1 (2018). https://doi.org/10.15392/bjrs.v6i1.332

[23] Maeda, Yukito, Akio Nagaki, Yoshihiro Komi, Nobukazu Abe, and Shinya Kashimura. "Evaluation of resolution correction in single photon emission computed tomography reconstruction method using a body phantom: Study of three different models." *Nihon Hoshasen Gijutsu Gakkai Zasshi* 71, no. 11 (2015): 1070-1079. https://doi.org/10.6009/jjrt.2015_JSRT_71.11.1070

[24] Barquero, Raquel, Hugo P. Garcia, Monica G. Incio, Pablo Minguez, Alexander Cardenas, Daniel Martínez, and Michael Lassmann. "131I activity quantification of gamma camera planar images." *Physics in Medicine & Biology* 62, no. 3 (2017): 909. https://doi.org/10.1088/1361-6560/62/3/909

[25] Mansour, Z., A. Mokhtar, A. Sarhan, M. T. Ahmed, and T. El-Diasty. "Quality control of CT image using American College of Radiology (ACR) phantom." *The Egyptian journal of Radiology and nuclear medicine* 47, no. 4 (2016): 1665-1671. https://doi.org/10.1016/j.ejrnm.2016.08.016

[26] Dewaraja, Yuni K., Michael Ljungberg, Alan J. Green, Pat B. Zanzonico, Eric C. Frey, Wesley E. Bolch, A. Bertrand Brill et al. "MIRD pamphlet no. 24: guidelines for quantitative 131I SPECT in dosimetry applications." *Journal of Nuclear Medicine* 54, no. 12 (2013): 2182-2188. https://doi.org/10.2967/jnumed.113.122390

[27] Peters, Steffie MB, Niels R. van der Werf, Marcel Segbers, Floris HP van Velden, Roel Wierts, Koos AK Blokland, Mark W. Konijnenberg, Sergiy V. Lazarenko, Eric P. Visser, and Martin Gotthardt. "Towards standardization of absolute SPECT/CT quantification: a multi-center and multi-vendor phantom study." *EJNMMI physics* 6 (2019): 1-14. https://doi.org/10.1186/s40658-019-0268-5

[28] Haghighatafshar, Mahdi, Elham Piruzan, Seyed Mohammad Entezarmahdi, Fatemeh Shekoohi-Shooli, and Mohammad Reza Parishan. "An applicable count rate saturation correction approach on gamma camera for I-131 labeled radiopharmaceuticals." *Results in Physics* 12 (2019): 1901-1904. https://doi.org/10.1016/j.rinp.2019.01.034

[29] Gregory, Rebecca A., Iain Murray, Jonathan Gear, Francesca Leek, Sarah Chittenden, Andrew Fenwick, Jill Wevrett et al. "Standardised quantitative radioiodine SPECT/CT imaging for multicentre dosimetry trials in molecular radiotherapy." *Physics in Medicine & Biology* 64, no. 24 (2019): 245013. https://doi.org/10.1088/1361-6560/ab5b6c